J. Fluid Mech. (2002), *vol.* 453, *pp.* 133–151.
DOI: 10.1017/S0022112001006796 Printed in the United Kingdom

Friction law for dense granular flows: application to the motion of a mass down a rough inclined plane

By OLIVIER POULIQUEN AND YOËL FORTERRE

IUSTI, Université de Provence, CNRS UMR 6595, 5 rue Enrico Fermi, 13453 Marseille cedex 13, France

(Received 22 January 2001 and in revised form 17 May 2001)

The problem of the spreading of a granular mass released at the top of a rough inclined plane was investigated. The evolution of the avalanche was measured experimentally from the initiation up to the deposit using a Moiré image-processing technique. The results are quantitatively compared with the prediction of an hydrodynamic model based on depth-averaged equations. In the model, the interaction between the flowing layer and the rough bottom is described by a non-trivial friction force whose expression is derived from measurements on steady uniform flows. We show that the spreading of the mass is quantitatively predicted by the model when the mass is released on a plane free of particles. When an avalanche is triggered on an initially static layer, the model fails in quantitatively predicting the propagation but qualitatively captures the evolution.

1. Introduction

Gravity-driven geophysical events sometimes involve the flow of a dry granular material. Landslides, rock avalanches and pyroclastic flows are examples of natural hazards where a granular mass flows down a slope. One of the problems is to predict the flow trajectory over the complex topography, the velocity and the runout distance in order to define a safety zone.

The difficulty in describing granular geophysical flows lies in the uncertainty in the constitutive equations for the flow of dry granular media (Rajchenbach 2000). Constitutive equations are known for rapid granular flows in a low-concentration regime, when the particles interactions are dominated by the collisions. For this regime, a kinetic theory can be developed based on the kinetic theory of dense gases taking into account the dissipation during the collisions (Haff 1983; Lun *et al.* 1984; Azanza, Chevoir & Moucheront 1999; Goldhirsch 1999). However, for dense flows when the particles not only undergo collisions but also friction and multicontact interactions with neighbouring particles, the kinetic approach is no longer valid. Some attempts have been made to incorporate into the kinetic theory which describes the collisional interactions, an empirical rate independent stress tensor in order to take the friction into account (Savage 1983; Johnson, Nott & Jackson 1990; Nott & Jackson 1992; Anderson & Jackson 1992). However, it is not clear that these approaches are valid for dense flows when multi-particle contacts are present. More recently, Savage (1998)

proposed an analysis for high-concentration flows based on a fluctuating plasticity model which has not yet been applied for flow down slopes. Another approach has been suggested by Mills *et al.* (1999, 2000) which is based on the idea that force chains are present in the media inducing a non-local formulation of the stresses.

A promising approach for describing unsteady and non-uniform flow on complex geometry such as geophysical flows, is the depth averaged Saint-Venant (1871) approach. In this framework, the material is assumed to be incompressible and the mass and momentum equations are written in a depth-averaged form. This analysis is valid under the assumption that the flowing layer is thin compared to its lateral extension, which is often the case for geophysical flows. Depth averaging allows us to avoid a complete three-dimensional description of the flow: the complex rheology of the granular material is incorporated in a single term describing the frictional stress that develops at the interface between the flowing material and the rough surface. Our goal in this paper is to propose an expression for this friction force based on experimental measurements, and to compare quantitatively the prediction of the depth-averaged approach with well-controlled experiments of granular avalanches.

Depth-averaged equations have been introduced in the context of granular flows by Savage & Hutter (1989). In their model, the interaction between the granular material and the rough surface is described by a simple friction law: the shear stress at the bottom is proportional to the normal stress, the coefficient of friction being a constant. The model works well when the surface of the plane is smooth enough: Savage, Hutter and coworkers were able to predict the motion and spreading of a granular mass on steep slopes in two and three dimensions (Savage & Hutter 1989; Gray, Wieland & Hutter 1999; Wieland, Gray & Hutter 1999). Experiments have been carried out also on curved beds (Greve & Hutter 1993; Greve, Koch & Hutter 1994; Koch, Greve & Hutter 1994), and the measurements agree relatively well with the prediction of the depth-averaged model. However, all the experiments have been carried out with high inclinations (higher than 40°) and with relatively smooth beds (typically 3 mm beads rolling on flat surfaces or sand paper).

For the flow of granular material on rough surfaces (where the roughness of the bed is of the order of the particle size) and for moderate inclinations, the description in terms of a simple solid friction no longer holds. This is shown by several experimental observations:

(i) It has been shown that steady uniform flows are observed in a range of inclination angles (Szuki & Tanaka 1971; Hungr & Morgenstern 1984; Vallance 1994; Ancey, Coussot & Evesque 1996; Pouliquen 1996*a*). This implies that the bed shear stress is not a simple solid friction but has a velocity dependence in order to balance the gravity for different inclinations.

(ii) The onset of flow on rough inclined planes is not described precisely by the simple solid friction law. According to this law, the flow is possible as soon as the inclination is higher than the friction angle. Experiments reveal a more complex behaviour; the onset of flow depends both on the inclination of the plane and on the thickness of the granular layer (Pouliquen & Renaut 1996; Daerr & Douady 1999; Pouliquen 1999*a*). A thin layer has more difficulty flowing than a thick one.

(iii) A hysteresis is observed between flowing and static states. A static layer of material resting on a rough surface will start flowing at a given threshold of the inclination. However, it will not stop before the slope decreases below a second threshold. In between these two angles there exist metastable states, where avalanches can be triggered by perturbations. The complex and rich dynamics of the avalanches has been recently studied by Daerr & Douady (1999) and Daerr (2001).

All these features cannot be captured by the simple solid friction assumption. The question we want to address in this study is: can we find a more realistic friction law within the depth-averaged framework which can capture the behaviour of thin granular layers on rough planes? Pouliquen (1999*a*) proposed an empirical friction law based on scaling properties measured for steady uniform flows. It has been shown that a depth-averaged description, taking into account this friction, predicts the steady shape of granular fronts propagating down a slope (Pouliquen 1999*b*). However, unsteady flows where static material starts to move, or moving material comes to rest, involve complex dynamics which are not *a priori* taken into account in the friction law. In the present study, our goal is to check to what extent the empirical friction law found for steady uniform flows can be used in the framework of the depth-averaged equations to quantitatively predict unsteady and non-uniform flows where deposits are formed and avalanches are triggered.

To this end, we have investigated two different experimental configurations. The first is the spreading of a granular mass released at the top of a rough inclined plane. The second is the release of a mass on a static layer of grains initially present on the rough plane. With the first configuration we can study how the material comes to rest and creates a deposit, whereas with the second we can study how static material is put into motion by flowing material. In both configurations the time evolution of the mass is measured and compared with the predictions of the depth-averaged model.

The experimental set-up and the measurement procedure are presented in § 2. In § 3, the depth-averaged model is described and the choice of the friction law is discussed. The results are presented in § 4. Discussion about the sensitivity of the model to the parameters is given in § 5 before concluding with the relevance and limits of the depth-averaged approach in § 6.

2. Experimental configurations

2.1. *Experimental set-up*

The experimental set-up is a 2 m long and 70 cm wide rough plane whose inclination θ can be controlled precisely. The surface is made rough by gluing one layer of particles onto the plane. The particles are glass beads 0.5 mm $\pm$0.04 in diameter. The first set of experiments consists in removing a spherical cap full of beads at the top of the plane. The released material then starts flowing down the slope, the mass spreads and ultimately stops leaving a tear-shaped deposit (figure 1*a*). Three roughly homothetic spherical caps were used: a small one ($r = 2.1$ cm, $R = 3.7$ cm), a medium one ($r = 3.1$ cm, $R = 6$ cm) and a large one ($r = 4$ cm, $R = 8$ cm, see figure 1(*a*) for the definition of r and R). In order to control precisely the amount of material present in the cap, the mass of beads poured into the cap is weighed before each run (62 g for the small cap, 231 g for the medium one, 524 g for the large cap).

In a second set of experiments the mass is released on the top of a layer of material already lying on the surface. The initially static layer is prepared by creating a steady uniform flow over the whole surface and by suddenly stopping the supply. In this case, a uniform deposit is created with a well-defined thickness h_{stop} depending only on the inclination θ (Pouliquen 1999*a*). The spherical cap is then carefully placed on the layer and filled with the beads. When the cap is suddenly removed, the mass spreads out putting into motion some of the initially static material, triggering an avalanching front.

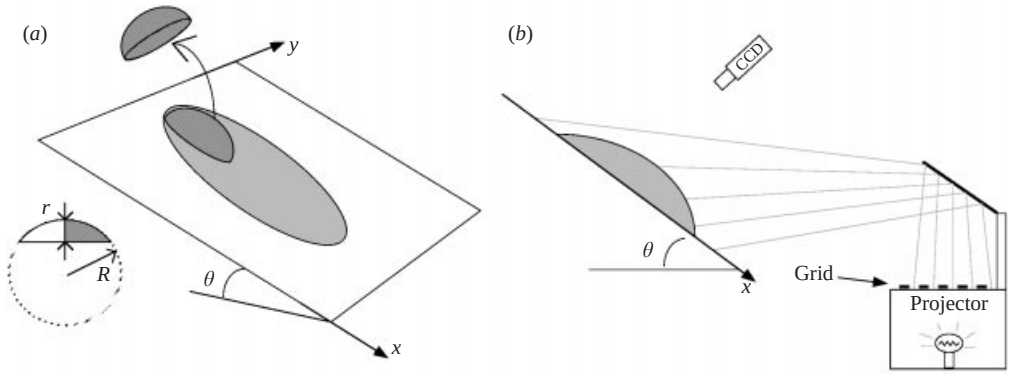

FIGURE 1. (*a*) Sketch of the experimental set-up. The spherical caps we used are part of a sphere of radius *R*. (*b*) Visualization method.

2.2. *Measurement method*

In order to measure precisely the time evolution of the granular mass, we have developed a method inspired by a Moiré method (Sansoni, Carocci & Rodella 1999). A grid pattern made of horizontal lines is projected on the plane by an overhead projector, as sketched in figure 1(*b*). The projection angle is small enough such that the presence of the granular mass on the surface induces a significant deformation of the grid (figure 2*b*). Pictures of the plane are recorded by a CCD camera positioned at the vertical of the plane. The local shift of the lines observed between the deformed pattern in the presence of a granular mass (figure 2*b*) and the initial regular pattern when the surface is flat (figure 2*a*) is proportional to the local thickness of the granular layer. In order to quantitatively obtain the thickness $h(x, y)$ we proceed as follows. The reference picture, figure 2(*a*), and the picture to be analysed, figure 2(*b*) are digitized which gives two real amplitudes $A_{ref}(x, y)$ and $A(x, y)$. The two-dimensional spatial Fourier transforms of both amplitudes are then computed. Both pictures being close to a regular pattern, the Fourier transforms are found to present well-defined peaks at the complex wavenumbers $(2\pi/\lambda, 0)$ and $(-2\pi/\lambda, 0)$, λ being the wavelength of the projected grid. For figure 2(*b*), the information about the slight deviation from the reference pattern induced by the granular mass is contained in the width of the peak. In order to extract the phase of the picture, the right-hand half of the wavenumber spectrum ($k_x > 0$) is used to reconstruct two complex amplitudes $A^c_{ref}(x, y)$ and $A^c(x, y)$. The phase $\phi_{ref}(x, y)$ and $\phi(x, y)$ of A^c_{ref} and A^c gives the phase of the pattern in figures 2(*a*) and 2(*b*). The thickness $h(x, y)$ is then simply proportional to the phase difference $\phi(x, y) - \phi_{ref}(x, y)$. The coefficient of proportionality is found by measuring the phase shift induced by a 1 cm thick plate. Figure 2(*c*) shows the contours of constant thickness given by the analysis.

The time evolution of the free surface of the mass $h(x, y, t)$ is obtained by analysing by this method each image of a movie recorded during the flow. The thickness measurement is estimated to be precise up to ± 0.3 mm. The phase measurement method breaks down when shadows are present behind the mass as in figure 2(*b*). In the region close to the shadow, the thickness is not correctly estimated and the contour of the deposit is not correct. The contour in this region is then estimated from direct visualization of the pictures. However, shadows are observed only at the first stage of the spreading when the layer is thick.

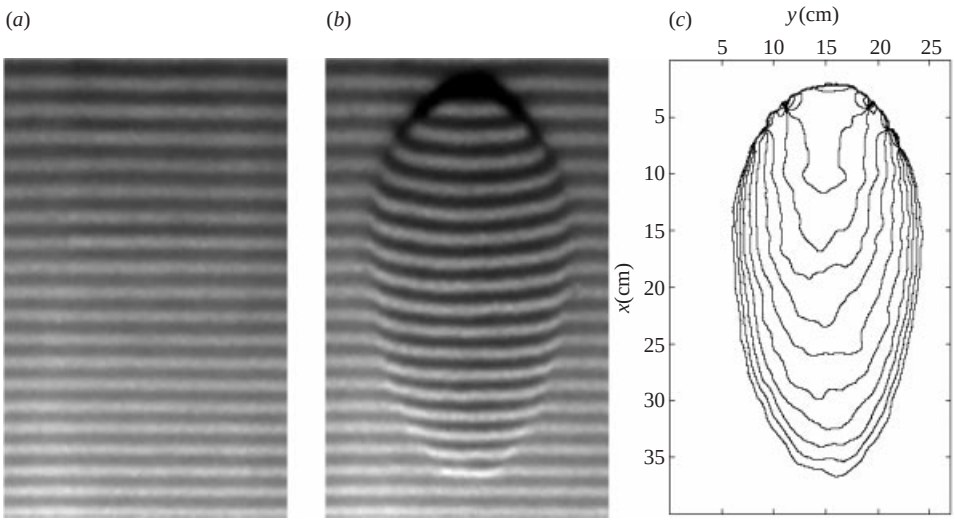

FIGURE 2. (*a*) Reference picture. (*b*) Picture to be analysed. (*c*) Contours of constant thickness every 0.5 mm given by the phase difference between (*a*) and (*b*).

3. Theoretical model

3.1. *Depth-averaged equations*

The use of depth-averaged equations to describe the flows under consideration here is motivated by the large aspect ratio of the granular mass: its lateral extension is large compare to the thickness of the layer.

More precisely, in order to derive the Saint-Venant equations we assume that the variation of the flow takes place on lengths much larger than the thickness. Assuming, in addition, that the flow is incompressible and of constant density ρ, which is justified for the dense flow regime studied here (Savage & Hutter 1989), we obtain the depth-averaged mass and momentum conservations by integrating the full three-dimensional equations (Savage & Hutter 1989). The following equations are written in terms of the local thickness $h(x, y, t)$ and the depth-averaged velocity $\boldsymbol{u}(x, y, t) = u\boldsymbol{e}_x + v\boldsymbol{e}_y$:

$$\frac{\partial h}{\partial t} + \frac{\partial (hu)}{\partial x} + \frac{\partial (hv)}{\partial y} = 0, \tag{3.1}$$

$$\rho \left(\frac{\partial (h\boldsymbol{u})}{\partial t} + \alpha \nabla \cdot (h\boldsymbol{u} \otimes \boldsymbol{u}) \right) = \rho g h \cos\theta \left(\tan\theta \boldsymbol{e}_x - \mu(h, \|\boldsymbol{u}\|) \frac{\boldsymbol{u}}{\|\boldsymbol{u}\|} - K \nabla \cdot h \right). \tag{3.2}$$

Equation (3.1) is the mass conservation. Equation (3.2) is the momentum conservation where the acceleration is balanced by three forces. In the acceleration expression, the coefficient α is related to the assumed velocity profile across the layer. In the case of a plug flow, $\alpha = 1$, whereas for a linear profile $\alpha = \frac{4}{3}$. For the sake of simplicity, we will use $\alpha = 1$ in the following. The results are not sensitive to the choice of α, as we will discuss in § 5. The first force on the right-hand side is the gravity parallel to the plane which is the driving force. The second term is the shear stress at the base; it is opposed to the motion, and is written as a friction coefficient μ multiplied by the vertical normal stress $\rho g h \cos\theta$. The friction coefficient *a priori* depends on the local thickness h and the local velocity $\|\boldsymbol{u}\|$. The last term in (3.2) represents the pressure force linked to the thickness gradient. The coefficient K represents the ratio of the vertical normal stress to the horizontal one (Savage & Hutter 1989).

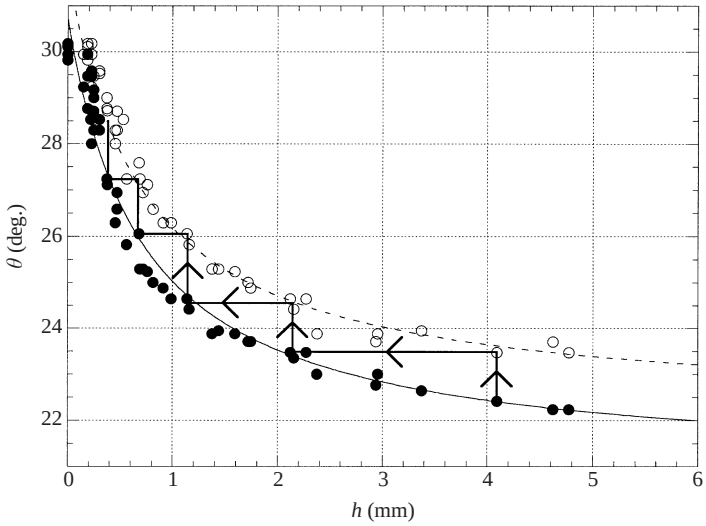

FIGURE 3. Variation of ○, the starting and ●, the stopping angles as a function of the thickness h. The arrows indicate the way they are measured: starting with a uniform layer h, θ is increased up to the point where an avalanche occurs. After the avalanche, h has a lower value, θ is increased again and so on. In the (h, θ) plane, we oscillate between the starting and stopping curves.

For quasi-static deformation this coefficient can be calculated from the standard Mohr–Coulomb plasticity model, as was done by Savage & Hutter (1989). However, for dense granular flows on rough surfaces, the material behaves more like a fluid. Numerical simulations tend to show that the vertical and horizontal normal stresses are equal (Prochnow, Chevoir & Albertelli 2000; Ertas *et al.* 2001). We then choose in the rest of the paper $K = 1$. This choice will be discussed in § 5.

In order to apply those equations to describe granular flows, we have to give the expression for the friction law $\mu(h, \|\boldsymbol{u}\|)$. No theory exists for determining the bottom shear stress in the dense regime. A first approximation is to consider the friction coefficient as constant. This approximation works well when the surface is smooth but does not predict correct results for flows on surface whose roughness is of the order of the particle diameter. Here, we use a more complex friction law based on previous experimental results obtained for steady uniform flows.

3.2. *The empirical friction law*

First, information about the friction mobilized in the thin granular layer is given by the onset of the flow. Experimental measurements have shown the existence of two critical angles. An initially static granular layer starts to flow when the inclination reaches a critical value θ_{start}. To stop the flow, we have to decrease the inclination to a lower angle θ_{stop}. The important result for the case of a layer on rough inclines is that the two angles are functions of the initial thickness h of the layer, as shown in figure 3 for the case of the glass beads used in our experiments. The two curves $\theta_{stop}(h)$ and $\theta_{start}(h)$ have the same shape but are translated from one another by roughly one degree. The same behaviour is observed with different materials on different roughness conditions (Pouliquen & Renaut 1996; Daerr & Douady 1999). In the following, we define the tangent of these angles $\mu_{start}(h) = \tan(\theta_{start}(h))$ and $\mu_{stop}(h) = \tan(\theta_{stop}(h))$. We show below that the knowledge of these two functions is sufficient to define the empirical friction law $\mu(h, \|\boldsymbol{u}\|)$ in the whole range of velocity and thickness.

Pouliquen 1999(*a*) showed that the friction coefficient $\mu(h, \|\boldsymbol{u}\|)$ is related to the function $\mu_{stop}(h)$ by the relation

$$\mu(h, \|\boldsymbol{u}\|) = \mu_{stop}\left(h\frac{\beta\sqrt{gh}}{\|\boldsymbol{u}\|}\right), \tag{3.3}$$

where β is a constant equal to 0.136 for glass beads, independent of the roughness conditions.

This non-trivial result comes from properties observed for steady uniform flows (Pouliquen 1999*a*). Steady uniform flows are controlled by the balance between friction and gravity which, according to (3.2), gives $\mu(h, \|\boldsymbol{u}\|) = \tan\theta$. To find the function μ, we simply have to know how the mean velocity $\|\boldsymbol{u}\|$ varies with the two control parameters h and θ. Taking the inverse of the relation $\|\boldsymbol{u}\|(h, \theta)$ gives $\mu(h, \|\boldsymbol{u}\|)$. Our measurements have shown that the mean velocity $\|\boldsymbol{u}\|$, the thickness of the granular layer h, and the inclination angle θ are related through:

$$\frac{\|\boldsymbol{u}\|}{\sqrt{gh}} = \beta\frac{h}{h_{stop}(\theta)}. \tag{3.4}$$

The function $h_{stop}(\theta)$ is the thickness of the deposit left by a steady uniform flow at the inclination θ. It is simply the inverse function of $\theta_{stop}(h)$. The expression of the friction coefficient (3.3) is then obtained by substituting θ by $\tan^{-1}(\mu)$ in the velocity expression (3.4).

However, the scaling law (3.4) is valid only for a Froude number defined as $Fr = \|\boldsymbol{u}\|/\sqrt{gh}$ greater than β; no steady uniform flow is observed with a lower Froude number, i.e. with a thickness h less than h_{stop}. It follows that the friction law (3.3) is only valid for $Fr > \beta$.

For $Fr < \beta$, we have no information about the friction law. Experiments on friction between solids (Heslot *et al.* 1994) or between a rough plate and a granular layer (Nasuno, Kudrolli & Gollub 1997) in the low-velocity regime have shown a complex and rich dynamics which is not yet fully understood. As a first approximation, the important point is that the friction coefficient first decreases when increasing the velocity, down to a minimum where it starts to increase. The velocity declining part is a source of instabilities (Heslot *et al.* 1994; Baumberger, Heslot & Perrin 1994). The fact that no steady uniform flow is observed for $Fr < \beta$ in our granular system suggests that the friction coefficient in this range decreases when increasing the Froude number. For $Fr < \beta$, we then assume that the friction coefficient $\mu(h, \|\boldsymbol{u}\|)$ tends to the static friction coefficient $\mu_{start}(h)$ when the velocity goes to zero. In between $Fr = 0$ and $Fr = \beta$, we simply extrapolate by a power function characterized by a power γ.

The final expression for the friction coefficient can then be written as follows (in terms of the thickness h and the local Froude number $Fr = \|\boldsymbol{u}\|/\sqrt{gh}$ instead of h and $\|\boldsymbol{u}\|$):

If $Fr > \beta$:

$$\mu(h, Fr) = \mu_{stop}\left(h\frac{\beta}{Fr}\right), \tag{3.5}$$

if $0 < Fr < \beta$:

$$\mu(h, Fr) = \left(\frac{Fr}{\beta}\right)^{\gamma}(\mu_{stop}(h) - \mu_{start}(h)) + \mu_{start}(h), \tag{3.6}$$

if $Fr = 0$:

$$\mu(h, 0) = \min(\mu_{start}(h), \|\tan\theta\mathrm{e}_x - K\nabla\cdot h\|). \tag{3.7}$$

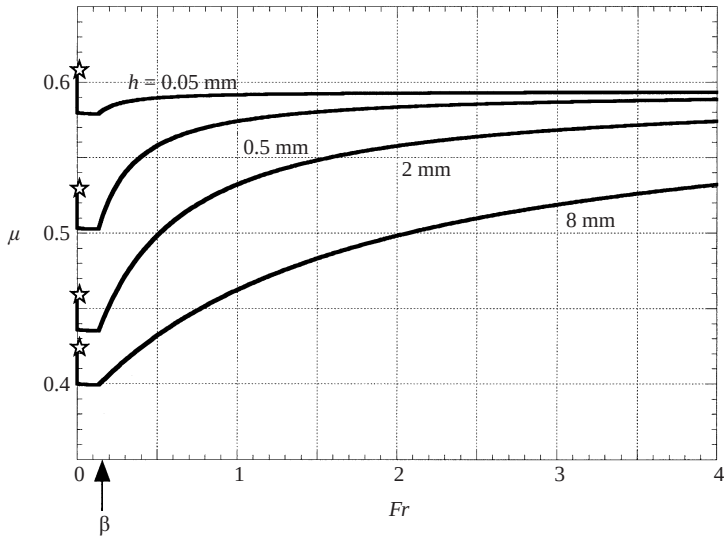

FIGURE 4. Friction coefficient $\mu(h, Fr)$ as a function of the Froude number $Fr = \|u\|/\sqrt{gh}$ for different thicknesses h. The stars gives the values for $Fr = 0$.

The last expression is just to ensure that, when the material is static, the friction balances the other forces exactly unless the total force reaches the threshold value given by the static friction coefficient.

The crucial point is that the above friction force is quantitatively determined by the two functions $\mu_{stop}(h)$ and $\mu_{start}(h)$ that can be measured easily in the experiments. For the glass beads used in the experiments, the best fits (figure 3) are given by:

$$\mu_{stop}(h) = \tan\delta_1 + (\tan\delta_2 - \tan\delta_1)\frac{1}{h/L + 1}, \tag{3.8}$$

$$\mu_{start}(h) = \tan\delta_3 + (\tan\delta_2 - \tan\delta_1)\frac{1}{h/L + 1}, \tag{3.9}$$

with $\delta_1 = 21^\circ$, $\delta_2 = 30.7^\circ$, $\delta_3 = 22.2^\circ$, and $L = 0.65\,\text{mm}$.

The only unknown coefficient in the friction law is the power γ of the extrapolation at low Froude numbers. We have checked that the predictions of the model are not sensitive to its value as long as γ is less than 10^{-2}. In the simulation, γ is chosen equal to 10^{-3}. The sensitivity to the value γ will be discussed in § 5. The friction coefficient $\mu(h, Fr)$ given by (3.5)–(3.9) is plotted in figure 4 as a function of the Froude number for different thicknesses. The reader has to keep in mind that only the part between $Fr = 0$ and $Fr = \beta$ is arbitrarily chosen. The value at $Fr = 0$ (start) and for $Fr > \beta$ is quantitatively given by the measurement of the function $\mu_{start}(h)$ and $\mu_{stop}(h)$. The discontinuity in the slope for $Fr = \beta$ is not physical and comes from the simple extrapolation we have chosen for the friction coefficient at low Froude number. We have checked that a smoother extrapolation around $Fr = \beta$ gives the same predictions.

The choice of the friction coefficient described above is such that it predicts the correct velocity for steady uniform flows, and the correct hysteresis for uniform layers (starting and stopping angles). The question is whether this friction law is sufficient to predict quantitatively more complex avalanching situations when it is introduced in the depth-averaged equations (3.2).

3.3. *Numerical methods*

In order to solve the depth-averaged equations, we have used two numerical methods depending on the configuration of interest. For the spreading of the mass on the empty plane, a Lagrangian method has been chosen as it allows us to treat easily parts where the thickness is zero. The method consists in discretizing the medium in elements which move and deform along with the flow. For the release of the mass on an initially static granular layer where shocks are likely to develop, we have written a shock capturing code based on a first-order Godunov scheme. Both numerical schemes are described in detail in the Appendix.

4. Results

4.1. *Release of a mass on a rough surface*

First, we have studied the spreading of the mass on a rough surface, free of particles. We have systematically measured the time evolution of the shape of the mass $h(x, y, t)$ for different inclinations and initial volumes and compared with the predicted evolution given by the simulation of the depth-averaged equations. No fit parameter exists in the simulation as soon as the functions $\mu_{stop}(h)$ and $\mu_{start}(h)$ are determined.

The time evolution of the spreading for the medium cap at $\theta = 23^\circ$ is presented in figure 5. The first row of figures shows contours of constant thickness measured in the experiments at five different times. When the material starts to flow, the mass rapidly spreads in both directions before it slowly stretches in the slope direction. The rear part of the mass stops (around $t = 2\,\mathrm{s}$), whereas the front forms a bump which propagates down the slope. The mass ultimately stops in a tear-like shape. This scenario is predicted well by the theory, as shown by the second row of figures in figure 5 giving the numerical predictions at the corresponding times. The last series of figures is a comparison of the thickness profiles along the longitudinal symmetry axis $y = 0$. Satisfactory agreement is obtained between theory and experiments from the initiation of the flow, up to the deposit. The presence of a thicker part flowing at the front when the rear part has already stopped ($t = 2.4\,\mathrm{s}$) is reproduced well by the theory.

The agreement remains correct for different inclinations, as shown in figure 6 which shows the deposits measured in the experiments and predicted by the simulations for different inclination angles. Although the shape of the deposit looks similar from one inclination to another, we have not been able to put in evidence any similarity shape solutions.

The effect of the initial mass has also been studied and the results are presented in figure 7. We have plotted the maximum width W and length L of the deposit for the three caps we used, as a function of the inclination. The lines correspond to the prediction of the model, the markers to the experimental observations. The agreement is good for the runout L of the deposit, whereas the lateral spreading W is overestimated by approximately 20%.

When the above results are compared with the prediction of the simple model using a constant friction coefficient (Savage & Hutter 1989), no deposit is predicted as soon as the inclination of the plane is higher than the friction angle. The whole material flows down the plane. For inclination lower than the friction angle, the pile spreads and stops when its free surface makes an angle with the horizontal equal to the friction angle. In any case, it is not possible with a constant friction law to predict a deposit whose free surface is parallel to the plane as observed in the experiments.

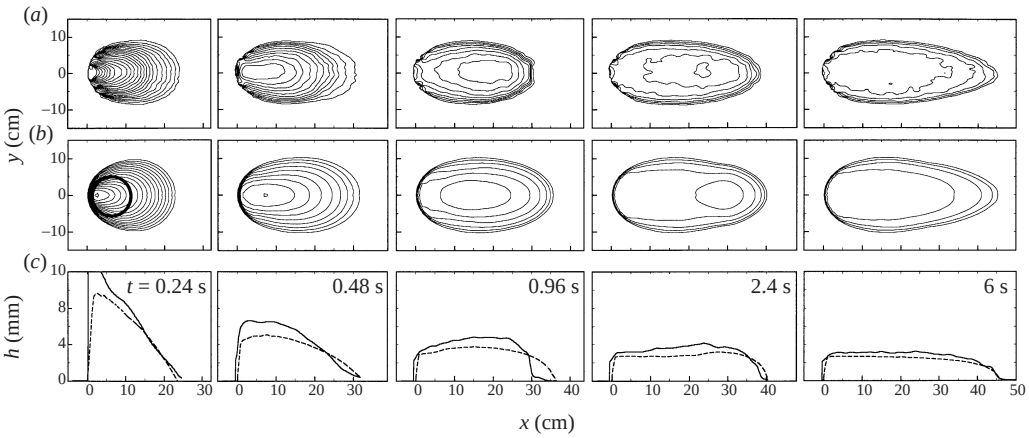

FIGURE 5. Time evolution of the granular mass for the medium cap $\theta = 23^\circ$. (a) Experiments. (b) Simulations; contour of constant thickness every 0.5 mm. (c) Thickness profiles along $y = 0$; ——, experiments; - - -, simulation. The bold circle on the first plot of the simulation represents the initial position of the cap.

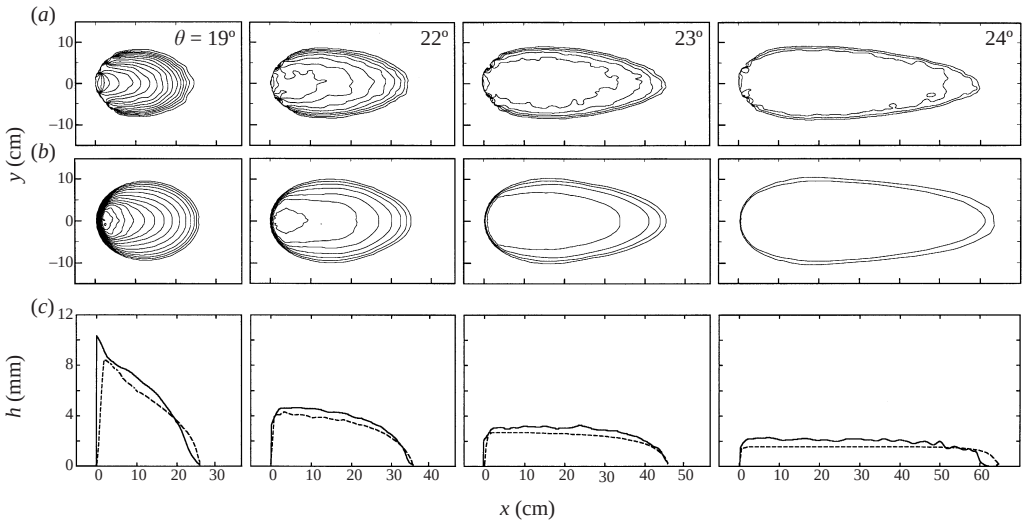

FIGURE 6. Comparison between (a) experiments and (b) simulations for the deposit obtained at different inclinations with the medium cap. Contours of constant thickness every 0.5 mm. (c) Thickness profiles, as figure 5.

4.2. *Release of a mass on an initially static layer of material*

The second set of experiments consists of releasing the mass on a static layer of granular material. We first prepare the layer by creating a steady uniform flow at an angle θ and by suddenly stopping the supply. A uniform deposit of thickness $h_{init} = h_{stop}(\theta)$ lies on the bed. We then carefully put the spherical cap on the layer and fill it with the beads. The mass is then released at $t = 0$ s. Results are presented in figure 8 for $\theta = 23^\circ$ and for the small cap. The first row corresponds to the experimental measurements of the free surface represented by contours of constant thickness. The second row are the corresponding predictions of the simulation. The

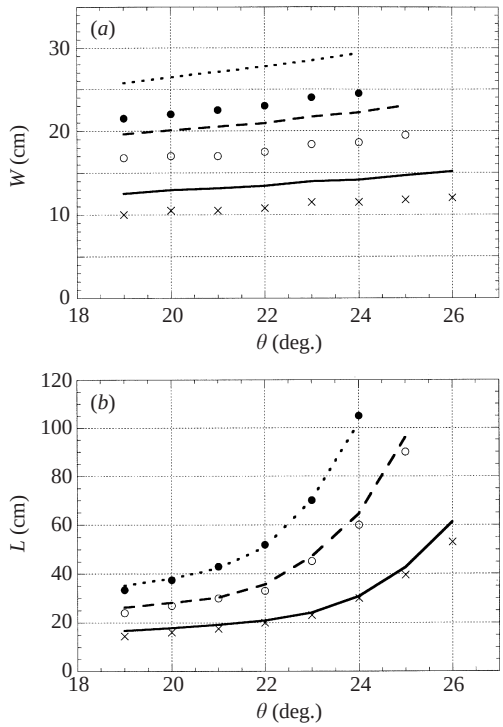

FIGURE 7. Comparison between experiments (markers) and simulation (lines) for (*a*) the maximum length L and (*b*) the width W of the deposit as a function of θ and for three different caps; $\cdots$, $\bullet$, large cap; $- - -$, $\circ$, medium cap; ——, $\times$, small cap.

third row of figures gives the thickness profiles along the longitudinal symmetry axis $y = 0$.

The mass when released rapidly spreads in both directions up to a point when it reaches a drop shape which propagates down the slope without significant deformations. This drop is a wave which puts into motion static material at the front and leaves static material at the rear. The front is very sharp and the thickness profile along $y = 0$ in the stationary regime is triangular as observed previously by Daerr (2001). This wave propagates faster than the material front in the previous deposit experiments described in § 4.1.

The simulation qualitatively predicts the same dynamics. The mass first spreads in both directions before reaching a roughly constant shape after about 4 s (not shown in figure 8) which propagates down the slope as a wave. In front of the wave, and behind it, the material is at rest. Whereas the rapid initial spreading ($t < 0.72$ s) seems to be quantitatively correctly predicted by the model, the long-time evolution is no longer in agreement with the experiments. The model predicts a saturated thickness at the front which is thinner than that observed in the experiment and the predicted propagation velocity is higher than the one observed. The front of the wave observed in the experiment is also more shocked than that predicted by the simulations. We have carried out experiments at different inclinations and with the other caps, which reveal the same discrepancy; the depth-averaged model always predicts a propagating wave which is too rapid and too thin compared to that observed in the experiments.

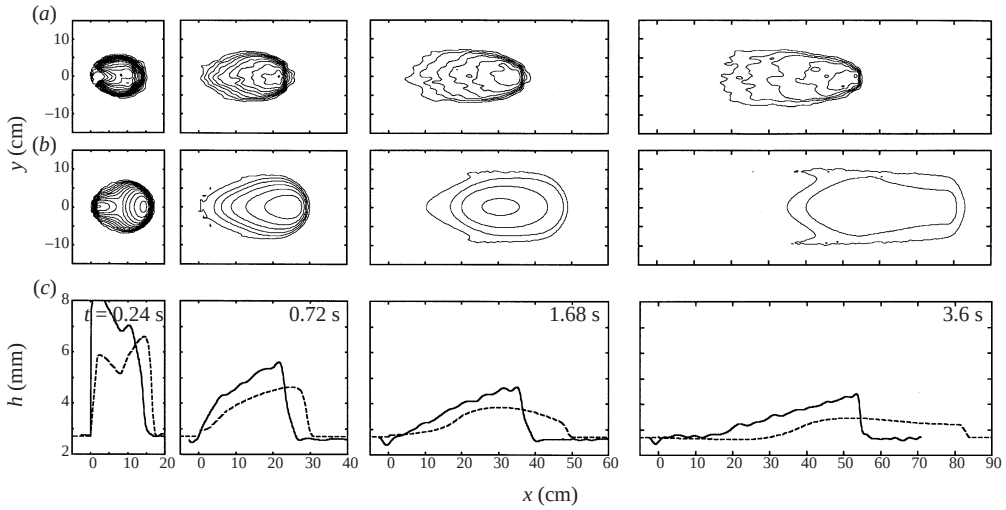

FIGURE 8. Time evolution of the granular mass released from the small cap on a initial layer of thickness $h_{init} = 2.7\,\text{mm}$, $\theta = 23^o$. (*a*) Experiments. (*b*) Simulations; contour of constant thickness every 0.3 mm (the external contour line is $h = 3\,\text{mm}$). (*c*) Thickness profiles along $y = 0$; ——, experiments; - - -, simulations.

5. Sensitivity of the model to the parameters

From the two configurations we have investigated, we can conclude that the depth-averaged model quantitatively predicts the formation of the deposit on the plane when the surface is free of particles, but fails to predict the correct avalanche propagation when a static layer is present. In order to understand the limits of the depth-averaged approach, we have studied the sensitivity of the simulation to the different parameters introduced in the model. We discuss below the role of the parameters we have not measured: α in the acceleration term, K in the pressure term, γ the power of the extrapolation at low Froude number.

5.1. *Role of* α

The parameter α in the acceleration term in (3.2) is obtained when integrating the three-dimensional conservation equations to derive the depth-averaged equation. It depends on the assumed velocity profile across the layer. In the simulation presented above, α was taken equal to 1, corresponding to a plug flow. For a linear profile α should be taken equal to $\frac{4}{3}$. For granular flow on a rough inclined plane, previous results suggest that the profile is closer to a linear profile than to a plug flow (Prochnow *et al.* 2000; Ertas *et al.* 2001). However, the results of the simulation are not very sensitive to the value of α. For example, simulations with $\alpha = \frac{4}{3}$ and $\alpha = 1$ for the case in figure 8 give a spatio-temporal evolution which differs only by a factor 2% for the thickness and velocities. The reason why the model is so insensitive can be understood by comparing the relative magnitude of the forces acting on the material. Except at the first instants of the spreading, the acceleration is negligible and the friction force balances the gravity forces. In other terms, inertia is negligible in the flow regime investigated in our experiments. This can be quantitatively estimated by locally measuring the ratio between the acceleration and the friction force defined by

the dimensionless number R_f:

$$R_f(x,y,t) = \frac{\| \tan\theta \boldsymbol{e}_x - \mu(h,\|\boldsymbol{u}\|)\dfrac{\boldsymbol{u}}{\|\boldsymbol{u}\|} - K\nabla\cdot h\|}{\mu(h,\|\boldsymbol{u}\|)}. \tag{5.1}$$

In the case of the deposit experiment of figure 5, R_f is maximum during the initial rapid spreading where it reaches the value 0.4 ($t < 0.5$ s) and rapidly decreases up to 0.02 everywhere for $t > 0.8$ s. In the case of the flow on a static layer (figure 8), R_f is less than 0.02 everywhere during the avalanche except at the front where material is put into motion. In this region, R_f reaches a higher value around 0.1. We can then conclude that inertial effects are negligible for the dense granular flow we are studying. The choice of α has then no significant influences on the prediction of the depth-averaged model for the configurations of interest in this study.

5.2. *Role of the pressure coefficient K*

A second parameter of the model is the pressure coefficient K in front of the thickness gradient term of (3.2). This coefficient represents the ratio of the horizontal normal stress to the vertical one. In the results presented above, we have used $K = 1$ corresponding to an isotropic pressure. This choice has been motivated by several numerical results showing a small difference between the two normal stresses (Prochnow *et al.* 2000; Ertas *et al.* 2001). Moreover, we observe that $K = 1$ gives the best agreement for the predicted deposits in § 4.1. An example of the prediction with another value of K is shown in figure 9. We have used the value $K = (1 + \sin^2\delta_1)/(1 - \sin^2\delta_1)$ corresponding to the Mohr–Coulomb prediction when the basal friction is equal to the internal friction coefficient taken equal to $\tan\delta_1$ (Savage & Hutter 1989). For our glass beads, we obtained $K = 1.29$. Using this value, the predicted deposit is wider and shorter than that experimentally observed. For the case of the flow on the static layer of figure 8, the higher value of K predicts also a larger spreading and does not influence the front propagation. Changing K does not provide better agreement for the propagation of the wave.

5.3. *Role of the power extrapolation γ*

The expression of the friction force in our model is quantitatively determined by the two functions $\mu_{stop}(h)$ and $\mu_{start}(h)$ except for the extrapolation at low Froude number. The extrapolation we have chosen is characterized by a power function with an exponent γ. In the simulation presented above, we have used $\gamma = 10^{-3}$. This low value ensures a rapid increase of the friction coefficient close to $Fr = 0$ (figure 4). No influence of γ is observed up to 10^{-2}. If we choose a larger power ($\gamma > 10^{-2}$), the depth-averaged model slightly underestimates the runout distance and overestimates the thickness of the deposit, especially at the rear where a small bump is predicted which is not observed. However, the effects are small. For example, for $\theta = 23^\circ$ the case $\gamma = 1$ predicts a runout distance $L = 41$ cm and a maximum deposit thickness of $h = 3.3$ mm whereas with $\gamma = 10^{-3}$ we obtain $L = 45$ cm and $h = 2.8$ mm.

For the case of the flow on a static layer, changing the value of γ does not significantly changes the front velocity in the figure 8.

In conclusion it seems that the discrepancy observed in figure 8 between the model and the measurement for the case of the kinematic wave moving on a static layer cannot be erased by tuning some of the parameters of the model.

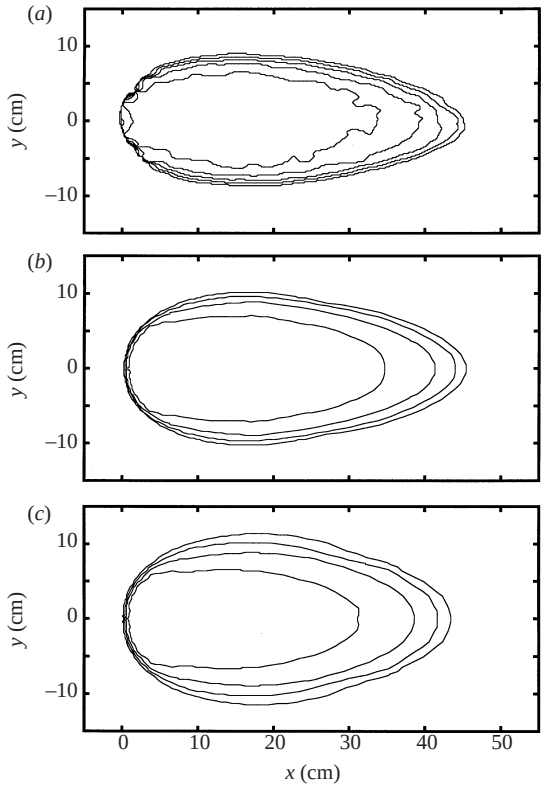

FIGURE 9. Deposits of the granular mass released from the medium cap $\theta = 23°$. (*a*) Experiment. (*b*) Simulation with $K = 1$. (*c*) Simulation with $K = 1.29$, the value given by the Mohr–Coulomb plasticity criterium.

6. Discussion and conclusion

We have shown in this paper that the flow of granular material along rough surfaces can be correctly described by introducing a relevant friction law in a depth-averaged description. The spreading of a mass on a rough slope free of particles is predicted quantitatively by the model from the release up to the deposit. The friction law introduced in the model for describing the interaction between the flowing granular layer and the rough surface is mainly quantitatively determined by the dependence of the stopping and starting angle with the thickness of the layer. Measuring these angles is enough to predict the velocity, the shape and the run-out of the mass.

However, we have shown in this study that the agreement is no longer correct when studying the release of the mass on a uniform granular layer initially static on the surface. The formation of a wave which puts into motion static material at the front and leaves material at the rear is predicted by the depth-averaged model, but the corresponding wave velocity and amplitude are not quantitatively in agreement with the measurements.

Several points could explain the discrepancy. First, the friction law we have used is too simple in the low-velocity regime and could be responsible for the wrong description of the front. However, we have not found a description which could capture the correct avalanche propagation. Secondly, at the front between the flowing part and the static part, the long-wave assumption breaks down. The thickness of

the layer varies on length scale of the order of the thickness. Thirdly, an underlying assumption in the depth-averaged equations is that the time variation of the properties at one point are slow enough that the velocity profile across the layer can be considered as fully developed. This assumption certainly breaks down for an avalanching front putting into motion some static material. The whole layer does not instantaneously start to flow but material at the free surface moves first, putting into motion the deeper layers. For such configurations, more complex approaches taking into account two layers, one for static grains, the other one for flowing grains, could be more relevant (Bouchaud *et al.* 1994; Boutreux, Raphael & de Gennes 1998; Douady, Andreotti & Daerr 1999). The question of the relevant friction law which should be used at the interface between the two layers is an open question. The one proposed in this study is perhaps not appropriate as it takes into account the influence of a rigid wall.

Geophysical flows are more complex than the simple avalanches of glass beads studied in this work. We can legitimately wonder to what extent similar approaches could be relevant for describing natural events. A first important difference concerns the nature of the material. Geophysical events involve complex heterogeneous granular material made of particles of various sizes ranging from micrometres to metres, often mixed with fluids. In such polydispersed material it is well known that segregation occurs with the large particles rising up to the free surface. The influence of the segregation process on the spreading of the mass and on the travelling distance of the avalanche are questions which represent works for future investigations.

Another difficulty for describing natural events is the complex topography. However, depth-averaged equations can be derived for non-uniform slopes, by introducing a local inclination that varies from one point to another. Works have been carried out in this direction on real topographies (Naaim Vial & Couture 1997; Heinrich *et al.* 2001). The results are promising, showing that the depth-averaged approach is certainly relevant when no mass exchange exists between the flowing mass and the substrate. However, the choice of the friction law for geophysical material remains an open issue.

This research was supported by the Ministère Français de la Recherche (ACI blanche 2018). Many thanks go to R. Saurel for his help in developing the Godunov code. Discussions with J. Misguisch were helpful for developing the Moiré method. We thank F. Ratouchniak for his technical assistance.

Appendix A. Lagrangian scheme

The Lagrangian method for simulating the depth-averaged equations is very similar to the one described by Wieland *et al.* 1999). The granular mass is discretized into a finite number of parallelepipedic elements which move and deform along with the flow. Velocities are defined at the node i of the grid and thickness at the middle of the element. The time evolution is obtained as follows:

(i) The position $\boldsymbol{x}_i^{t+1}$ of the node i at time $t+1$ is evaluated by:

$$\boldsymbol{x}_i^{t+1} = \boldsymbol{x}_i^t + \Delta t \boldsymbol{u}_i^t,$$

where $\boldsymbol{u}_i^t$ is the velocity.

(ii) The thickness at the centre of the element is computed using the mass conservation:

$$h_i^{t+1} = V_i / S_i^{t+1},$$

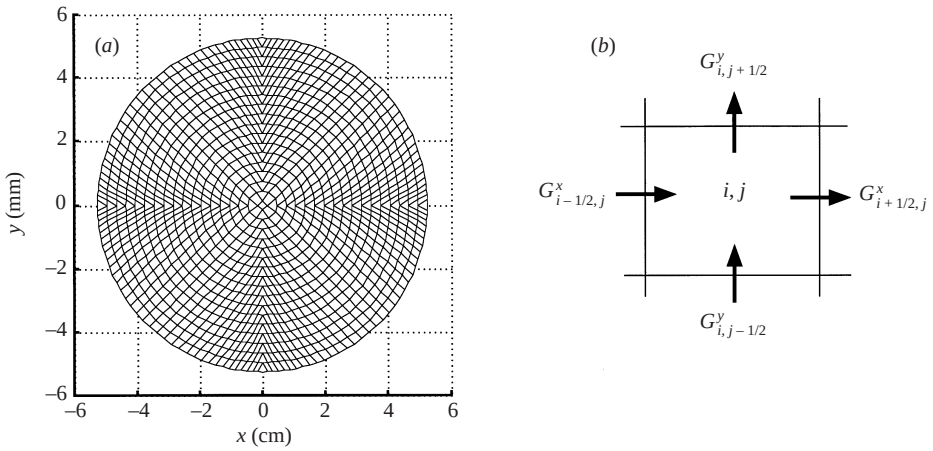

FIGURE 10. (*a*) Initial position of the elements for the Lagrangian simulation for the medium cap. (*b*) Sketch of one cell and the corresponding horizontal and vertical fluxes for the Godunov scheme.

where V_i is the volume of element i which remains constant during the flow, and S_i^{t+1} is the surface of element i given by the new positions of the four corners of the element.

(iii) The velocities are updated as follows:

$$\boldsymbol{u}_i^{t+1} = \boldsymbol{u}_i^t + \Delta t \boldsymbol{F}_i^t,$$

where $\boldsymbol{F}_i^t$ are the forces at the node corresponding to the right-hand side of (3.2). To evaluate $\boldsymbol{F}_i^t$, we need to know the thickness and thickness gradient at the nodes. They are evaluated using standard finite-element interpolation (Grandin 1986). Note that with this Lagrangian formulation, the coefficient α in the acceleration term in (3.2) is equal to 1.

The 35×35 elements are initially disposed as in figure 10(*a*) and the thickness is initialized to fit the spherical cap used in the experiments. Initial velocities are zero and the time increment is set to 5×10^{-4} s.

Appendix B. Shock capturing scheme

We have developed a second code to model the flow on an initially static material. It is based on a first-order Godunov scheme (Godunov 1959) in order to be able to correctly capture shock propagation. Equations (3.1) and (3.2) are rewritten in a conservative form:

$$\frac{\partial \boldsymbol{U}}{\partial t} + \frac{\partial \boldsymbol{G}^x}{\partial x} + \frac{\partial \boldsymbol{G}^y}{\partial y} = \boldsymbol{F},$$

where $\boldsymbol{U}$, $\boldsymbol{G}^x$, $\boldsymbol{G}^y$ and $\boldsymbol{F}$ are vectors depending on the thickness h and longitudinal and transverse velocities u and v as follows:

$$\boldsymbol{U} = \begin{pmatrix} h \\ hu \\ hv \end{pmatrix}, \ \boldsymbol{G}^x = \begin{pmatrix} hu \\ \alpha hu^2 + Kh^2 \\ \alpha huv \end{pmatrix}, \ \boldsymbol{G}^y = \begin{pmatrix} hv \\ \alpha huv \\ \alpha hv^2 + Kh^2 \end{pmatrix},$$

$$\boldsymbol{F} = \begin{pmatrix} 0 \\ \rho g h \cos\theta \left(\tan\theta - \mu(h, Fr) \dfrac{u}{\sqrt{u^2 + v^2}} - K \dfrac{\partial h}{\partial x} \right) \\ \rho g h \cos\theta \left(-\mu(h, Fr) \dfrac{v}{\sqrt{u^2 + v^2}} - K \dfrac{\partial h}{\partial y} \right) \end{pmatrix}.$$

The data are discretized on a regular grid. Knowing the vector $\boldsymbol{U}^t_{i,j}$ at time t and at the point (i, j), we compute its value at time $t + \Delta t$ as follows:

$$\boldsymbol{U}^{t+\Delta t}_{i,j} = \boldsymbol{U}^t_{i,j} - \frac{\Delta t}{\Delta x} \left(\boldsymbol{G}^x_{i+1/2,j} - \boldsymbol{G}^x_{i-1/2,j} \right) - \frac{\Delta t}{\Delta y} \left(\boldsymbol{G}^y_{i,j+1/2} - \boldsymbol{G}^y_{i,j-1/2} \right) + \boldsymbol{F}_{i,j} \Delta t,$$

where $\boldsymbol{G}^x_{i+1/2,j}$ and $\boldsymbol{G}^y_{i,j+1/2}$ are the horizontal and vertical fluxes calculated at the frontier between cells (figure 10*b*). We use the HLL (Harten, Lax & van Leer 1983) approximation to compute the fluxes at the frontier from the fluxes at the centre of the cell:

$$\boldsymbol{G}^x_{i+1/2,j} = \frac{C^{x,l}{}_{i+1/2,j} \boldsymbol{G}^x_{i,j} - C^{x,r}{}_{i+1/2,j} \boldsymbol{G}^x_{i+1,j} + C^{x,l}{}_{i+1/2,j} C^{x,r}{}_{i+1/2,j} (\boldsymbol{U}^t_{i+1,j} - \boldsymbol{U}^t_{i,j})}{C^{x,l}{}_{i+1/2,j} - C^{x,r}{}_{i+1/2,j}},$$

$$\boldsymbol{G}^v_{i,j+1/2} = \frac{C^{y,l}{}_{i,j+1/2} \boldsymbol{G}^y_{i,j} - C^{y,r}{}_{i,j+1/2} \boldsymbol{G}^y_{i,j+1} + C^{y,l}{}_{i,j+1/2} C^{y,r}{}_{i,j+1/2} (\boldsymbol{U}^t_{i,j+1} - \boldsymbol{U}^t_{i,j})}{C^{y,l}{}_{i,j+1/2} - C^{y,r}{}_{i,j+1/2}}.$$

The wave velocities are estimated by the following choice proposed by Davis (1988):

$$C^{x,l}{}_{i+1/2,j} = \min(0, \alpha u_{i+1,j} - c^x_{i+1,j}, \alpha u_{i,j} - c^x_{i,j}),$$
$$C^{x,r}{}_{i+1/2,j} = \max(0, \alpha u_{i+1,j} + c^x_{i+1,j}, \alpha u_{i,j} + c^x_{i,j}),$$
$$C^{y,l}{}_{i,j+1/2} = \min(0, \alpha u_{i,j+1} - c^y_{i,j+1}, \alpha u_{i,j} - c^y_{i,j}),$$
$$C^{y,r}{}_{i,j+1/2} = \max(0, \alpha u_{i.j+1} + c^y_{i,j+1}, \alpha u_{i,j} + c^y_{i,j}),$$

with $c^x_{i,j} = \sqrt{(\alpha^2 - \alpha) u^2_{i,j} + 2K h_{i,j}}$ and $c^y_{i,j} = \sqrt{(\alpha^2 - \alpha) v^2_{i,j} + 2K h_{i,j}}$.

The simulations presented in the paper have been obtained with $\Delta x = \Delta y = 0.15\,\text{cm}$ and $\Delta t = 5 \times 10^{-4}\,\text{s}$.

REFERENCES

Ancey, C., Coussot, P. & Evesque, P. 1996 Examination of the possibility of a fluid-mechanics treatment of dense granular flows. *Mech. Cohesive-Frictional Mater.* **1**, 385–403.

Anderson, K. G. & Jackson, R. 1992 A comparison of the solutions of some proposed equations of motion of granular materials for fully developed flow down inclined planes. *J. Fluid Mech.* **241**, 145–168.

Azanza, E., Chevoir, F. & Moucheront, P. 1999 Experimental study of collisional granular flows down an inclined plane. *J. Fluid Mech.* **400**, 199–227.

Baumberger, T., Heslot, F. & Perrin, B. 1994 Crossover from creep to inertial motion in friction dynamics. *Nature* **367**, 544–546.

Bouchaud, J. P., Cates, M., Prakash, J. R. & Edwards, S. F. 1994 A model for the dynamics of sandpile surfaces. *J. Phys. Paris* I **4**, 1383–1410.

Boutreux, T., Raphael, E. & de Gennes, P. G. 1998 Surface flows of granular material: a modified picture for thick avalanches. *Phys. Rev.* E **58**, 4692–4700.

Daerr, A. 2001 Dynamical equilibrium of avalanches on a rough plane. *Phys. Fluids* **13**, 2115–2124.

Daerr, A. & Douady, S. 1999 Two types of avalanche behaviour in granular media. *Nature* **399**, 241–243.

Davis, S. F. 1988 Simplified second order Godunov type methods. *SIAM J. Sci. Statist Comput* **9**, 445–473.

Douady, S., Andreotti, B. & Daerr, A. 1999 On granular surface flow equations. *Eur. Phys. J.* B **11**, 131–142.

Ertas, D., Grest, G. S., Halsey, T. H., Levine, D. & Silbert, E. 2001 Gravity-driven dense granular flows. Preprint cond-mat/0005051.

Godunov, S. K. 1959 A finite difference method for the numerical computation of discontinuous solutions of the equations of fluid dynamics. *Maths USSR Sb.* **47**, 357–393.

Goldhirsch, I. 1999 Scales and kinetics of granular flows. *Chaos* **9**, 659–672.

Grandin, H. 1986 *Fundamentals of the Finite Element Method*. Macmillan.

Gray, J. M. N. T., Wieland, M. & Hutter, K. 1999 Gravity-driven free surface flow of granular avalanches over complex basal topography. *Proc. R. Soc. Lond.* A **455**, 1841–1874.

Greve, R. & Hutter, K. 1993 Motion of a granular avalanche in a convex and concave curved chute: experiments and theoretical predictions. *Phil. Trans. R. Soc. Lond.* A **342**, 573–600.

Greve, R., Koch, T. & Hutter, K. 1994 Unconfined flow of granular avalanches along a partly curved surface: I. Theory. *Proc. R. Soc. Lond.* A **445**, 399–413.

Haff, P. K. 1983 Grain flow as a fluid-mechanical phenomenon. *J. Fluid Mech.* **134**, 401–430.

Harten A., Lax, P. D. & van Leer, B. 1983 On upstream differencing and Godunov type schemes for hyperbolic conservation laws. *SIAM Rev.* **25**, 33–61.

Heinrich, P., Boudon, G., Komorowski, J. C., Sparks, S. & Herd, H. 2001 Numerical simulation of the December 1997 debris avalanche in Montserrat, Lesser Antilles. Preprint.

Heslot, F., Baumberger, T., Perrin, B., Caroli, B. & Caroli, C. 1994 Creep, stick-slip, and dry-friction dynamics: experiments and a heuristic model. *Phys. Rev.* E **49**, 4973–4987.

Hungr, O. & Morgenstern, N. R. 1984 Experiments on the flow behavior of granular materials at high velocity in an open channel. *Géotechnique* **34**, 405–413.

Johnson, P. C., Nott, P. & Jackson, R. 1990 Frictional–collisional equations of motion for particulate flows and their application to chutes. *J. Fluid Mech.* **210**, 501–535.

Koch, T., Greve, R. & Hutter, K. 1994 Unconfined flow of granular avalanches along a partly curved surface: II. Experiments and numerical simulations. *Proc. R. Soc. Lond.* A **445**, 415–435.

Lun, C. K. K., Savage, S. B., Jeffrey, D. J. & Chepurniy, N. 1984 Kinetic theories for granular flow: inelastic particles in Couette flow and slightly inelastic particles in a general flowfield. *J. Fluid Mech.* **140**, 223–256.

Mills, P., Loggia, D. & Tixier, M. 1999 Model for a stationary dense granular flow along an inclined wall. *Europhys. Lett.* **45**, 733–738.

Mills, P., Tixier, M. & Loggia, D. 2000 Influence of roughness and dilatancy for dense granular flow along an inclined wall. *Eur. Phys. J.* E **1**, 5–8.

Naaim, M., Vial, S. & Couture, R. 1997 Saint Venant approach for rock avalanches modeling. In *Multiple Scale Analyses and Coupled Physical Systems: Saint Venant Symposium*. Presse de l'École Nationale des Ponts et Chaussees, Paris.

Nasuno, S., Kudrolli, A. & Gollub, J. P. 1997 Friction in granular layers: hysteresis and precursors. *Phys. Rev. Lett.* **79**, 949–953.

Nott, P. & Jackson, R. 1992 Frictional–collisional equations of motion for granular materials and their application to flow in aerated chutes. *J. Fluid Mech.* **241**, 125–144.

Pouliquen, O. 1999*a* Scaling laws in granular flows down rough inclined planes. *Phys. Fluids* **11**, 542–548.

Pouliquen, O. 1999*b* On the shape of granular fronts down rough inclined planes. *Phys. Fluids* **11**, 1956–1958.

Pouliquen, O. & Renaut, N. 1996 Onset of granular flows on an inclined rough surface: dilatancy effects. *J. Phys. Paris* II **6**, 923–935.

Prochnow, M., Chevoir, F. & Albertelli, M. 2000 Dense granular flows down a rough inclined plane. In *Proc. XIIIth Intl Congr. on Rheology, Cambridge, UK*.

Rajchenbach, J. 2000 Granular flows. *Adv. Phys.* **49**, 229–256.

de Saint-Venant, A. J. C. 1871 Théorie du mouvement non-permanent des eaux, avec application aux crues des rivières et à l'introduction des marées dans leur lit. *C. R. Acad. Sci. Paris* **73**, 147–154.

Sansoni, G., Carocci, M. & Rodella, R. 1999 3D vision based on the combination of gray code

and phase shift light projection: analysis and compensation of the systematic errors. *Appl. Opt*. **31**, 6565–6573.

Savage, S. B. 1983 Granular flows down rough inclines – review and extension. In *Advances in Micromechanics of Granular Materials* (ed. J. T. Jenkins, M. Satake *et al*.). Elsevier.

Savage, S. B. 1998 Analyses of slow high-concentration flows of granular materials. *J. Fluid Mech.* **377**, 1–26.

Savage, S. B. & Hutter, K. 1989 The motion of a finite mass of granular material down a rough incline. *J. Fluid Mech.* **199**, 177–215.

Suzuki, A. & Tanaka, T. 1971 Measurement of flow properties of powders along an inclined plane. *Ind. Engng. Chem. Fundam.* **10**, 84–91.

Vallance, J. W. 1994 Experimental and field studies related to the behavior of granular mass flows and the characteristics of their deposits. PhD thesis, Michigan Technological University.

Wieland, J. M., Gray, J. M. N. T. & Hutter, K. 1999 Channelized free-surface flow of cohesionless granular avalanches in a chute with shallow lateral curvature. *J. Fluid Mech.* **392**, 73–100.